Non-catalytic After-treatment for Diesel Particulates Using Carbon-fiber Filter and Experimental Validation

by

Kazuhiro YAMAMOTO, Fumihiro FUJIKAKE, Kenta MATSUI
Department of Mechanical Science and Engineering, Nagoya University
Furo-cho, Chikusa-ku, Nagoya, Aichi 464-8603, JAPAN

ABSTRACT

Recently, the stricter diesel emission standards have been setting and an after-treatment of exhaust gas is needed. In this study, as a potential non-catalytic system, the after-treatment using a carbon-fiber filter was investigated, where soot particulates are burned by an electric heater. In the vehicle tests, the experimental validation for our proposed system was conducted, where the soot volume fraction and particle size distribution in diesel exhaust gas were measured. Since the filter was attached to the exhaust pipe, the filter backpressure increased with higher soot emission. Thus, the performance of the filter was evaluated under the same pressure condition. It is confirmed that, the soot emission is greatly reduced by trapping the diesel soot. In addition, the particle number concentration is smaller, so that most of soot particulates are trapped and burned inside the filter. However, in the after-treatment process, particulates less than 30 nm are newly formed. In experiments, the information on the soot oxidation process was limited, and the numerical simulation was performed to investigate temperature field and soot oxidation rate in the filter. It is found that the continuous regeneration is largely promoted by increasing the filter wall temperature. Hence, it is necessary to pay more attention on the effect of filter wall temperature on the particle size for more reduction of smaller particulates.

1. Introduction

Diesel vehicles have features of low fuel consumption and high durability, and can reduce the release of CO_2 (greenhouse gas). However, particulate matters (PM) including soot are exhausted from diesel vehicles, which cause environmental problems such as adverse health effects [1]. Recently, much attention worldwide has been given to the influence of nanoparticles in the atmosphere. It should be noted that, in the current regulations, we do not have to consider very fine nanoparticles, because their mass is very low. However, if the regulation is set based on particle number, these particulates should be removed as well. Indeed, the Euro VI in 2013-14 will be set for the regulations of PM from the conventional weight basis to a particle number basis [2,3]. Thus, in addition to an improvement of in-cylinder combustion, an after-treatment technology with a diesel particulate filter (DPF) is needed [3-7].

Although many types of filters have been developed, most of commercially available DPF are ceramic honeycomb filters. When the exhaust gas passes through DPF, PM is accumulated and removed in the thin filter wall. The filtration efficiency could be over 99% [5,8]. One problem is the occurrence of an increase in filter backpressure due to collection of PM. A subsequent worsening of fuel efficiency and engine output has been reported [4-6]. In order to prevent these disadvantages, a continuously regenerating DPF has

been proposed, which traps and oxidizes PM simultaneously [3,7,9]. There are three types of filter regeneration; thermal regeneration, catalytic regeneration, and aerodynamic regeneration [4]. Although the aerodynamic regeneration is conducted by using compressed air, the removal of deposited PM may not be enough. In addition, the thermal durability of existing platinum catalyst-supported DPF is inadequate, which means that the catalyst may be damaged by PM oxidation and the filter may also be cracked. Since platinum is a rare metal, an establishment of new PM treatment technologies without recourse to catalysts could be urgently required. Hence, it is necessary to develop a non-catalytic after-treatment of diesel particulates with highly thermal durability.

Figure 1 shows a schematic of our after-treatment system, with a direct photograph of a filter [10]. The exhaust gas is forced to pass through the filter, and particulates are removed by the conical-shaped carbon-fiber filter with enough thermal durability. Needless to say, the carbon-fiber has been widely used in aerospace industry. The average porosity is approximately 0.8. The porosity of the conventional ceramic filter is from 0.4 to 0.5 [3-7]. Then, the filter backpressure of the carbon-fiber filter is expectedly lower.

In order to prevent clogging of the filter, an electric heater is used during vehicle running. Dependent on the situation, air is introduced to promote PM oxidation without catalysts, which was not applied in this

study. Consequently, the continuous regeneration is achieved. However, in the vehicle tests, only the pressure drop (filter backpressure) and the exhaust gas emission are measured, and the information is limited [5,8,10,11]. It is difficult to observe how PM is deposited and oxidized inside the carbon-fiber filter. So far, we have succeeded in developing a numerical scheme for the soot deposition and oxidation using the lattice Boltzmann method (LBM) [9,12-15].

In the present paper, vehicle tests are conducted to evaluate the proposed system using a laser-induced incandescence (LII) for diesel soot measurements. Additionally, to identify conditions required for continuous regeneration, the after-treatment with the carbon-fiber filter is numerically simulated. In order to consider the phenomenon inside the actual filter, the inner structure of the filter is obtained using an X-ray computed tomography (CT) technique, and the tomography-assisted simulation is performed using LBM.

Fig.1

2. Experimental setup

2.1. LII system

To detect diesel nanoparticles, we used the LII technique. It is one of the laser diagnostics with abilities to measure very low soot concentration [16-21], ensuring that we could validate the after-treatment system.

The advantages of LII are as follows: (1) soot concentration can be measured with high resolution of time and space; (2) because of non-intrusive measurement, the effect of LII on the measuring field can be minimized [22]; and (3) since two-dimensional measurement by a laser-sheet can be performed, the spatial distribution is obtained.

Figure 2 shows an experimental setup. In the LII system, soot concentration and soot particle size are generally evaluated based on the signals from incandescence of soot particulates irradiated by the high-intensity laser. A frequency doubled (532nm, 10Hz) Nd:YAG laser was used for the light source. In order to conduct outdoor experiments in vehicle tests, a compact laser device (Inlite produced by Continuum Inc., USA) was used. Its laser head is only 84 mm (H) × 94 mm (W) × 323 mm (L), and its weight including the power supply section is only 35 kg; i.e., this device is convenient for portable use. The maximum output was 125 mJ/pulse at 532 nm. The energy fluctuation from pulse to pulse was negligible. Since the soot concentration in exhaust gas was uniform, a laser beam instead of the laser sheet was used to improve signal-to-noise ratio (SNR). Its beam diameter was 2 mm, and the LII signal was obtained along the beam line in **Fig. 2**. Images were detected by a CCD camera with an image intensifier (Hamamatsu Photonics K. K., Japan). A band-pass filter (FWHM = 10 nm) with the central wavelength at 400 nm was installed in front of

ICCD camera [17,18,20]. The pixel number of the camera was 1024 × 1024, and the image area was 34 mm × 34 mm. Silica glass was attached to the camera to protect the lens and optical filter from exhaust gas. The gate width of the image intensifier was set at 50 ns for noise reduction. The signals were recorded by a personal computer for data analysis.

Fig.2

Next, the calibration procedure of LII signal is explained [16,21]. The LII signal in flames was measured using a coaxial jet diffusion flame burner, converted into soot volume fraction. The burner size and flow conditions were the same in Ref. 16. **Figure** 3 shows the relationship between LII signal and soot volume fraction of jet diffusion flame. The fuel was methane. The fuel velocity was 4 cm/s in condition 1, and 7.78 cm/s in condition 2. For both cases, the air velocity was 7.9 cm/s. We obtained LII signals by changing the axial distance from the burner, compared with the reported soot volume fraction [16,22]. Although the LII signal of luminous flame was varied further downstream due to the flickering behavior, it was confirmed that the LII signal is proportional to the soot volume fraction.

The primary particle size was measured with a LII200 (Artium Technologies Inc., USA) [23], which was validated by a sampling system with SMPS (Scanning Mobility Particle Sizer, TSI Model 3034).

Fig.3

2.2. Vehicle test

Using the above-mentioned apparatus, the soot emission and particle size exhausted from an actual vehicle were measured. The diesel vehicle was a Mazda MPV. The type was KD-LVLW produced in 1995, and its engine displacement was 2499 cc. The standard ultra-low-sulfur diesel fuel was used, with 10 ppm or less of sulfur. As shown in **Fig. 1**, the electric heater implemented with a usual 12V battery was used in the after-treatment system. The measuring area was 10 mm after the exhaust pipe outlet. The same experimental approach in our previous study was applied by keeping the same load [8]. Various driving conditions were tested at different engine speed, which was adjusted to the following 7 levels: 900, 1500, 2000, 2500, 3000, 3500, and 4000 rpm. The temperature and pressure of the exhaust gas were monitored before entry into and after leaving the filter. The temperatures of the exhaust gas and the filter wall were set to be 400 and 700 ℃ [24], respectively. By using two sets of thermocouples, these temperatures were monitored. Since the heat conduction of the carbon-fiber filter was very high, the temperature inside the filter wall was uniform. However, except for the temperature measurement, it was difficult to observe the soot oxidation phenomena inside the filter by experiments. Then, by changing the filter wall temperature, we examined the soot oxidation process (see section 4.5).

As explained before, due to particulate deposition, the filter will become clogged to increase the filter backpressure. Especially, there is an initial filter backpressure without any particle deposition. In this measurement, to presume a change in filter backpressure, many sets of packing with various orifice diameters were used, inserted into the middle of the exhaust pipe using flanges. **Figure 4** shows an example of an actual attachment. The original diameter of the exhaust pipe was 58 mm (ϕ 58), and the backpressure was changed by inserting the packing with an orifice diameter of ϕ 15, 18, 20, 26, or 30 mm. Then, we can validate our filtration system under the same pressure condition (see section 4.3). For each test, a set of 300 images was recorded.

Fig.4

2.3. Carbon-fiber filter and X-ray CT measurement

As shown in **Fig. 1,** the exhaust gas is forced to pass through the filter to trap diesel particulates. The housing electrical heaters were placed to raise filter wall temperature. **Figure 5** shows the image of inner structure of the carbon-fiber filter obtained by a three-dimensional X-ray CT technique. SiC composite material with enough thermal durability was used, and its typical fiber diameter was 10 μm. Dotted box in **Fig. 1** shows roughly a view field of **Fig. 5**. Non-destructive nature of the CT technique allows visualization of

inner structure needed for simulation [9,12-15]. The thickness (L) of the filter was 3.1 mm, and the spatial resolution of CT measurement was 13.3 μm/pix, which was the grid size in the simulation. Comparing with our previous work [14], the larger grid size was chosen, simply because the filter thickness was larger. In our preliminary measurement, the size and number of grid system were changed. It was confirmed that the grid size of 13.3 μm was enough to construct the carbon-fiber structure. The part of the filter enclosed by the dotted line in **Fig. 5** was used in the simulation.

Fig.5

3. Numerical method

Previously, we have proposed a numerical scheme to simulate the combustion field by LBM [25]. So far, the flow and the soot oxidation process inside the filter have been well simulated [10,12-15]. For the continuously regenerating trap system, both soot deposition and oxidation must be considered simultaneously. Since the numerical scheme for soot oxidation has been found in our references, the approach to describe the soot deposition model is explained here.

The soot concentration in the gas phase is determined by convection, diffusion, and chemical reaction [10,15]. That is, the soot is transported by the convective motion of gaseous mixture and the mass diffusion

caused by the concentration gradient. Also, the soot is consumed by the oxidation. The LB equation for soot mass fraction is,

$$F_{C,\alpha}(\boldsymbol{x}+\boldsymbol{e}_\alpha\delta_t,\ t+\delta_t)-F_{C,\alpha}(\boldsymbol{x},\ t)=-\frac{1}{\tau_C}[F_{C,\alpha}(\boldsymbol{x},\ t)-F^{eq}_{C,\alpha}(\boldsymbol{x},\ t)]+w_\alpha Q_C \qquad (1)$$

where F_C is the distribution function for soot mass fraction, $\boldsymbol{e}_\alpha$ is the unit vector in lattice coordinate, δ_t is the time step, and τ_C is the relaxation time related with diffusion coefficient. The source term, Q_C, is determined by the soot oxidation rate, and the equilibrium distribution function, $F_{C,\alpha}^{eq}$, is given by

$$F^{eq}_{C,\alpha}=w_\alpha Y_{C,g}\left\{1+3\frac{(\boldsymbol{e}_\alpha\cdot\boldsymbol{u})}{c^2}+\frac{9}{2}\frac{(\boldsymbol{e}_\alpha\cdot\boldsymbol{u})^2}{c^4}-\frac{3}{2}\frac{\boldsymbol{u}\cdot\boldsymbol{u}}{c^2}\right\} \qquad (2)$$

where w_α is the numerical constant in equilibrium formula in LB model. The local velocity vector of $\boldsymbol{u}$ is obtained by the distribution function of flow field [12-14,25]. The mass fraction of soot in gas phase is obtained by the sum of the distribution function as $Y_{C,g} = \Sigma F_{C,\alpha}$. It should be noted that soot in gas phase accumulates on the filter surface or the soot layer. The soot deposition is described by the modified particle deposition model. Our approach is similar to the particle deposition model using deposition efficiency [26]. Different from Lagrangian approach through the equation of motion, individual particles are not considered.

Instead, the soot concentration is monitored, so that we do not have to consider the complex geometry of nanoparticles [17,21]. The mass fraction of deposited soot is given by

$$Y_{C,s}(\boldsymbol{x},\ t+\delta_t) = \sum_{\alpha} F_{C,\alpha}(\boldsymbol{x},\ t)\cdot P_D + Y_{C,s}(\boldsymbol{x},\ t) \qquad (3)$$

where $Y_{C,s}$ is the mass fraction of deposited soot treated as the solid phase, and P_D is the soot deposition probability, which controls the amount of deposited soot to the filter [10,15]. If P_D is unity, soot is thoroughly deposited at the filter surface without reflection. Else, some of particles are bounced back and transported downstream. As the soot deposition is continued, the soot mass fraction sometime becomes unity. When this limit is reached, the solid site is piled up, and the deposited soot region is treated as non-slip wall, which implies a dynamic change of boundary condition for fluid. In our preliminary experiments, we determined the value of P_D. For carbon-fiber filter, P_D was 0.001 [15]. Then, we adopted this value in the simulation.

The calculation domain and coordinate in the simulation are shown later (see **Fig. 10a**). The calculation domain is 5.19 mm × 0.53 mm × 0.53 mm. The total number of grids is 391 (N_x) × 41 (N_y) × 41 (N_z), with grid size of 13.3 μm, corresponding to the spatial resolution of the CT measurement. As explained in **Fig. 5**, the part of CT data was inserted at the center of the calculation domain. For the boundary

condition, the inflow boundary was adopted at the inlet. The inflow velocity is 1 m/s. The temperature of exhaust gas is 400℃. The soot mass fraction is 4.54×10^{-5}, corresponding to the value in experiments [15]. Oxygen concentration is 10% in volume (0.113 in mass fraction), which is a typical value of diesel exhaust gas [14,27]. At the side wall, the slip boundary condition was adopted, considering the symmetry. At the outlet, the pressure was constant, and the gradient of scalar such as temperature and mass fraction was set to be zero. On the filter surface or the deposited soot layer, the non-slip boundary condition was adopted. For the reaction scheme, an over-all one step reaction proposed by Lee et al. was adopted [28].

4. Results and discussion

4.1. Observation of filter surface

To discuss the filter structure after deposition of diesel particulates, the filter surface was observed with a laser beam microscope (VK-9500; Keyence Corporation, Japan). **Figure 6** shows images of the filter surface before and after deposition in vehicle tests, respectively. The engine speed was 1500 rpm and the temperature of exhaust gas was 400 ℃. Since we could not mark the view field of filter, these images show different area with the same size. In order to observe the state after deposition, the filter regeneration by

electric heating was not performed. As shown in **Fig. 6a**, carbon-fibers are clearly observed. When soot adheres to the filter surface in **Fig. 6b**, the fiber diameter becomes larger than doubling their previous size. Based on CT measurement, the average porosity in **Fig. 6a** is approximately 0.8 before deposition, and it changes to be 0.4 after deposition. Thus, without the filter regeneration process, the filter is easily clogged by the soot deposition, and consequently, the filter backpressure largely increases.

Fig.6

4.2. Backpressure with changing engine speed

The vehicle test was conducted to evaluate the proposed system. Here, the backpressure (ΔP) was monitored at different engine speed (R). **Figure 7** shows the relationship between R and ΔP, obtained by equipping a packing with orifice diameter of ϕ 15−30 mm or the filter. As already explained, the diameter of exhaust pipe was 58 mm, and the condition without orifice was shown simply by ϕ 58 mm. It is found that the backpressure increases at higher engine speed. This tendency appears more pronounced as the orifice diameter is smaller. Additionally, ΔP is increased when the carbon-fiber filter is equipped, corresponding to the value with a packing of ϕ 26 mm.

Fig.7

4.3. Soot volume fraction

The soot volume fraction in diesel exhaust gas was measured by the LII technique. As already explained in section 2.1, the LII signal was converted to soot volume fraction. Results are shown in **Fig. 8**. The soot concentration in exhaust gas was uniform, and the data derivation in LII measurement was within 10 %. Only mean values using 300 images are plotted. As seen in this figure, the soot volume fraction is almost constant when R is in the range of 1500−2500 rpm, and increases above 2500 rpm. This tendency is more apparent when a packing with smaller orifice is equipped. By comparing these results with the backpressure in **Fig. 6**, an increase in the soot volume fraction is revealed as ΔP increases.

Fig.8

It has been reported that more soot is formed in diffusion flames under high pressure [29−32]. Therefore, in addition to the soot aggregation, the soot emission may increase due to the higher backpressure. Alternatively, the higher back-pressure could make the scavenging process less effective in cylinder with valve system of engine, yielding a lower air-fuel ratio to promote soot formation. Since ΔP with a packing of ϕ 26 mm is the same as that with the filter, it was possible to evaluate the performance under the same pressure condition. Apparently, the soot volume fraction was greatly decreased by equipping the filter, and the validity of the proposed system was confirmed.

4.4. Soot particle size

To study further, the primary soot particle size was investigated, using the filter and the packing of ϕ 26 mm. **Figure 9** shows particle size distributions of primary soot at R = 1500 and 2500 rpm. The size distribution of ϕ 26 mm well corresponds to the typical distribution of diesel exhaust gas [33]. Interestingly, the particle number is largely decreased and the particle size is smaller due to the filtration. However, smaller particulates less than 30 nm are newly formed. This could be because soot particulates become smaller due to surface burning [34]. That is, when carbon particles are oxidized, the particle size is firstly decreased. Then, parts of the chain structure are thought to be torn, thereby generating smaller particles. Since the emission of these nanoparticles may cause a health concern, more improvements of the system are needed.

Fig.9

4.5. Simulation of after-treatment process

A numerical simulation was performed to investigate the phenomena inside the carbon-fiber filter in detail. **Fig. 10a** shows the computational domain with coordinate system, where x is the flow direction of exhaust gas. The simulated 3D profile of deposited soot is shown in **Fig. 10b**. The filter wall temperature (T_w) was set at 700ºC. In **Fig. 10b**, the color profile in x-y plane expresses the distribution of soot mass fraction in

gas phase, the purple three-dimensional contour expresses the deposited soot, and the gray contour expresses the filter. As shown in this figure, the soot concentration gradually decreases inside the filter, and a large amount of soot is deposited on the surface of carbon-fiber.

Fig.10

Figure 11 shows distributions of soot mass fraction in gas phase, temperature, and reaction rate. These are obtained in *x*-*y* plane at the center of the computational domain at T_w = 700ºC. As seen in **Fig. 11a**, the soot concentration is almost zero at the filter outlet. Along the filter wall, the temperature rise due to the soot combustion is not constant in **Fig. 11b**, and 110ºC is the maximum at this condition. In downstream, the temperature is almost constant, because the soot oxidation rate is small. The oxygen concentration is not varied much, because the soot concentration in exhaust gas is very low. In **Fig. 11c**, the reaction rate is large on the carbon-fiber filter, and it is very small in gas phase. Therefore, it is considered that soot in exhaust gas is firstly deposited, and then oxidized on the carbon-fiber filter.

Fig.11

Next, the effect of filter wall temperature is examined. **Figure 12** shows the profile of deposited soot along the flow direction. The filter wall temperatures are 700, 1200, 1400 ºC. It is found that, at the area near the filter inlet (1 mm < x < 1.5 mm), the soot concentration tends to decrease regardless of T_w. Therefore, in this region, the half of soot in exhaust gas is deposited. In the range of 1.5 mm < x, the large difference

between three profiles is observed, because more soot is oxidized at higher T_w. The soot is oxidized completely at T_w = 1200 and 1400 ℃. Hence, the soot oxidation is largely promoted by increasing the filter wall temperature [4]. In the future study, we need to pay more attention on the effect of filter wall temperature or air injection on the particle size to reduce the emission of smaller particulates.

5. Conclusions

In this study, the exhaust gas after-treatment using the carbon-fiber filter was investigated as a potential non-catalytic system. In experiments, the vehicle test was conducted to monitor the soot volume fraction and particle size. In order to realize the same pressure condition with the filter, the exhaust pipe was equipped with packing of different orifice diameter. In addition, the numerical simulation was performed. The following conclusions were drawn:

(1) When the engine speed is increased, the soot volume fraction is increased, resulting in higher backpressure. Based on observation of filter surface without electric heating, soot adheres to carbon fibers, and the diameter becomes larger than doubling their thickness. Because of soot deposition, the average porosity is decreased approximately from 0.8 to 0.4.

(2) By equipping the filter, the backpressure is higher, which could increase the soot emission in exhaust gas. The backpressure with the filter is the same as that with the packing of ϕ 26 mm. When the performance of the filter is evaluated under the same pressure condition, the performance of the proposed system can be evaluated.

(3) Since the size and number concentration of particulates are largely decreased, most of soot particles are trapped and burned inside the filter. However, smaller particulates less than 30 nm are newly formed. This could be because the soot aggregation collapses to form smaller nanoparticles in the combustion process.

(4) Inside the filter, the soot in exhaust gas is firstly deposited, and then oxidized on the carbon-fiber filter. As the filter wall temperature is higher, the soot oxidation is largely increased. Thus, the filter wall temperature is the key to promote the soot oxidation process for more reduction of smaller particulates.

References

[1] I. M. Kennedy, Proc. *Combust. Inst.* 31 (2007) 2757-2770.

[2] *Official Journal of the European Union*, Regulation (EC) No. 595/2009, July 18 (2009).

[3] T. V. Johnson, *SAE Technical Paper* 2010-01-0301 (2010) 16-29.

[4] G. C. Koltsakis, A. M. Stamatelos, *Prog. Energy Combust. Sci*. 23 (1997) 1-39.

[5] E. Wirojsakunchai, E. Schroeder, C. Kolodziej, et al., *SAE Technical Paper* 2007-01-0320 (2007).

[6] D. Timo, J. Uwe, P. Manfred, *Chemical Engineering Journal* 135 (2008) 49-55.

[7] T. V. Johnson, *SAE Technical Paper* 2011-01-0304 (2011) .

[8] K. Tsuneyoshi, O. Takagi, and K. Yamamoto, SAE 2011 World Congress 2011-01-0817 (2011) 297-305.

[9] J. R. Warner, D. Dobson, G. Cavataio, *SAE Int. J. Fuels Lubr.* 3(1) (2010) 149-164.

[10] K. Yamamoto, S. Satake, H. Yamashita, N. Takada, and M. Misawa, *the European Physical Journal* 171 (2009) 205-212.

[11] B. Wehner, U. Uhrner, S. Lowis, M. Zallinger, and A. Widensohler, *Atmospheric Environment* 43 (2009) 1235-1245.

[12] K. Yamamoto, N. Takada, and M. Misawa, *Proc. Combust. Inst*. 30 (2005) 1509-1515.

[13] K. Yamamoto, S. Satake, H. Yamashita, N. Takada, and M. Misawa, *Mathematics and Computers in Simulation* 72 (2006) 257-263.

[14] K. Yamamoto, S. Oohori, H. Yamashita, and S. Daido, *Proc. Combust. Inst*. 32 (2009) 1965-1972.

[15] K. Yamamoto, K. Yamauchi, N. Takada, M. Misawa, H. Furutani, and O. Shinozaki, *Philosophical Transactions A (The Royal Society, London)*, 369 (2011) 2584-2591.

[16] C. R. Shaddix, K. C. Smyth, *Combust. Flame* 107 (1996) 418-452.

[17] R. L. Vander Wal, K. A. Jensen, M. Y. Choi, *Combust. Flame* 109 (1997) 399-414.

[18] S. M. Lee, S. S. Yoon, and S. H. Chung, *Combust. Flame* 136 (2004) 439-500.

[19] Y. Xin, and J. P. Gore, *Proc. Combust. Inst*. 30 (2005) 719-726.

[20] S. S. Yoon, S. M. Lee, S. H. Chung, *Proc. Combust. Inst.*, 30 (2005) 1417-1424.

[21] K. C. Oh, H. D. Shin, *Fuel* 85 (2006) 615-624.

[22] K. Kohse-Hoinghaus and J. B. Jeffries, Applied combustion diagnostics, Taylor & Francis, New York, 2002, pp.252-286.

[23] http://www.artium.com/index.html

[24] D. S. Park, J. U. Kim, E. S. Kim, *Combust. Flame* 114 (1998) 585-590.

[25] K. Yamamoto, X. He, and G. D. Doolen, *J. Statistical Physics*, Vol. 107, Nos.1/2 (2002) 367-383.

[26] X. Wang, C. You, R. Liu, R. Yang, *Proc. Combust. Inst*. 33 (2011) 2821-2828.

[27] J. Oi-Uchisawa, A. Obuchi, A. Ogata, R. Enomoto, S. Kushiyama, Applied Catalysis B 21 (1999) 9-17.

[28] K. B. Lee, M. W. Thring, and J. M. Beer, *Combust. Flame* 6 (1962) 137-145.

[29] W. L. Flower, C. T. Bowman, *Proc. Combust. Inst*. 21 (1988) 1115-1124.

[30] K. A. Thomson, Ö. L. Gülder, E. J. Weckman, R. A. Fraser, G. J. Smallwood, D. R. Snelling, *Combust. Flame* 140 (2005) 222-232.

[31] D. S. Bento, K. A. Thomson, Ö. L. Gülder, *Combust. Flame* 145 (2006) 765-778.

[32] H. I. Joo, and Ö. L. Gülder, *Proc. Combust. Inst* 32 (2009) 769-775.

[33] D. B. Kittelson, *J. Aerosol Sci.* 29 (1998) 575-588.

[34] J. Song, M. Alam, A. L. Boehman, and U. Kim, *Combust. Flame* 146 (2006) 589-604.

Figure captions

Fig. 1 A schematic of after-treatment system. Dotted box roughly shows a view field of Fig. 4.

Fig. 2 Experimental setup for LII system.

Fig. 3 Soot volume fraction and LII signal of jet diffusion flames are shown. Fuel is methane. The fuel velocity is 4 cm/s at condition 1, and 7.78 cm/s at condition 2. For both cases, air velocity is 7.9 cm/s.

Fig. 4 Exhaust pipe and flange with packing.

Fig. 5 Image of inner structure of carbon-fiber filter by an X-ray CT technique.

Fig. 6 Images of filter surface; (a) before deposition, (b) after deposition.

Fig. 7 Backpressure equipped with packing with different orifice diameter or filter.

Fig. 8 Soot volume fraction equipped with packing with different orifice diameter or filter.

Fig. 9 Particle size distributions of primary soot equipped with packing with ϕ26 or filter; (a) R=1500 rpm, (b) R = 2500 rpm.

Fig. 10 (a) Computational domain with coordinate system, (b) 3D distribution of deposited soot inside filter. Profile in x-y plane expresses distribution of soot mass fraction in gas phase. Purple color-shaded contour expresses deposited soot. Gray contour expresses filter.

Fig. 11 Distributions of (a) soot mass fraction in gas phase, (b) temperature, (c) reaction rate; T_w=700℃.

Fig. 12 Distributions of deposited soot at T_w=700, 1200, 1400℃.

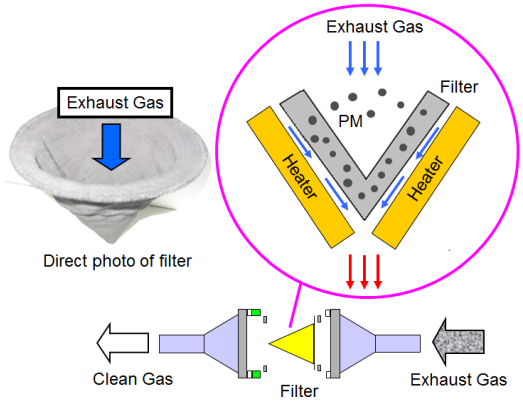

Fig. 1 A schematic of after-treatment system.
Dotted box roughly shows a view field of Fig. 4.

[Word Count] = (52+10)*2.2*1 + 17 (caption) = 154 words

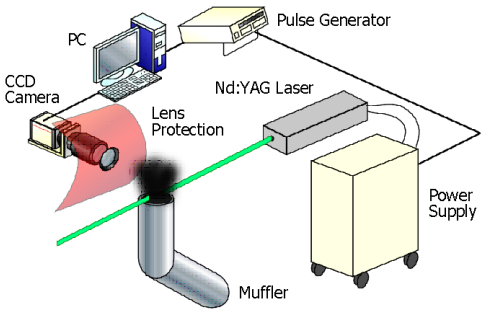

Fig. 2 Experimental setup for LII system.

[Word Count] = (39+10)*2.2*1 + 6 (caption) = 114 words

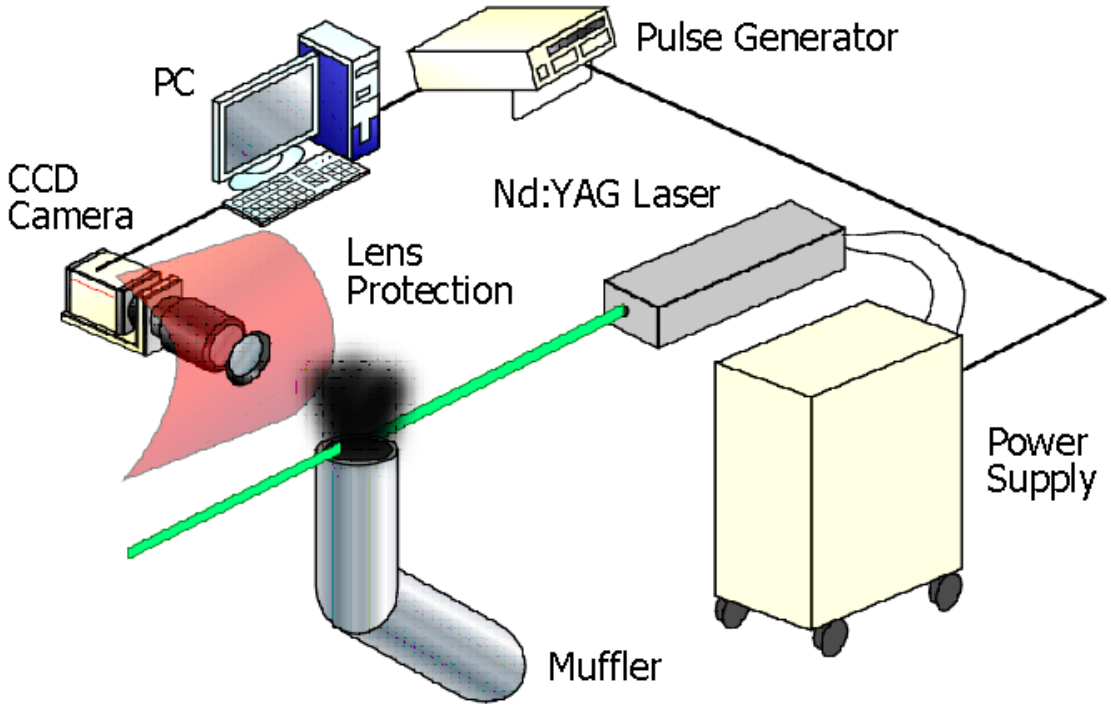

Fig. 2 (enlarged)

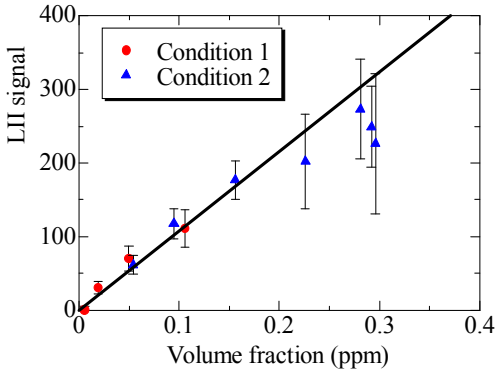

Fig. 3 Soot volume fraction and LII signal of jet diffusion flames are shown. Fuel is methane. The fuel velocity is 4 cm/s at condition 1, and 7.78 cm/s at condition 2. For both cases, air velocity is 7.9 cm/s.

[Word Count] = (46+10)*2.2*1 + 40 (caption) = 164 words

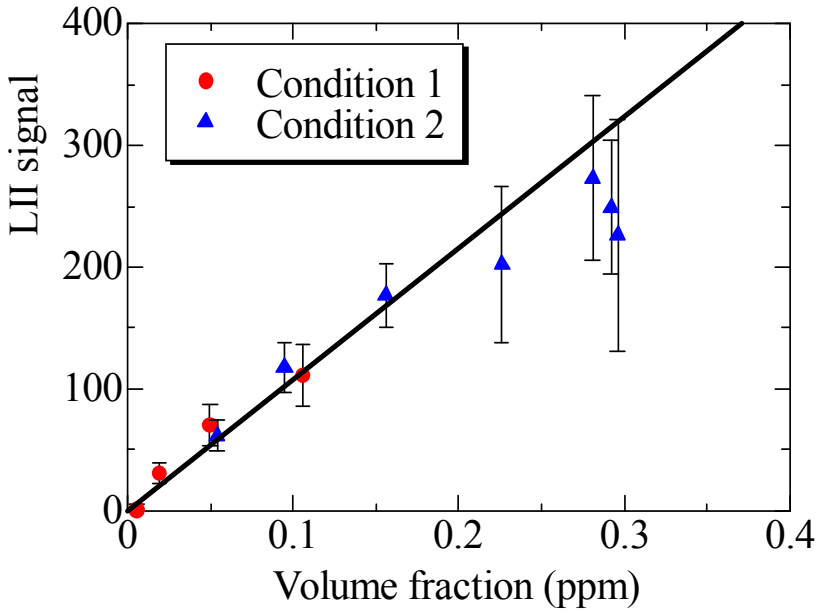

Fig. 3 (enlarged)

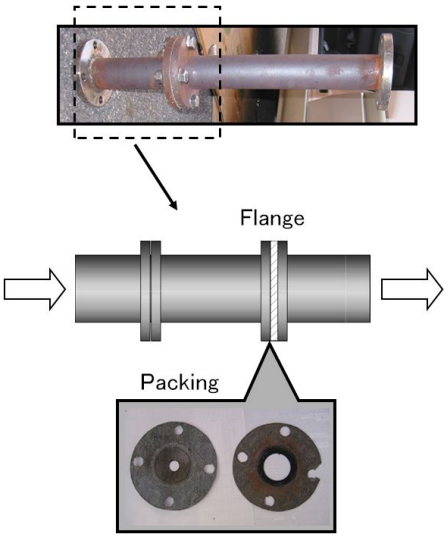

Fig. 4 Exhaust pipe and flange with packing.

[Word Count] = (67+10)*2.2*1 + 7 (caption) = 177 words

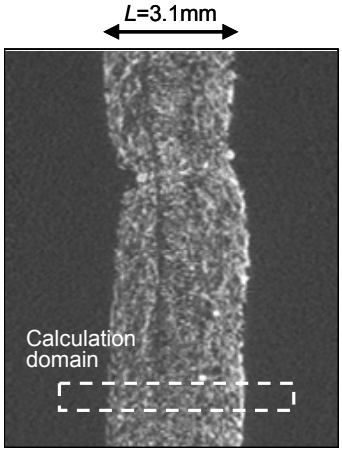

Fig. 5 Image of inner structure of carbon-fiber filter
by an X-ray CT technique.

[Word Count] = (52+10)*2.2*1 + 14 (caption) = 151 words

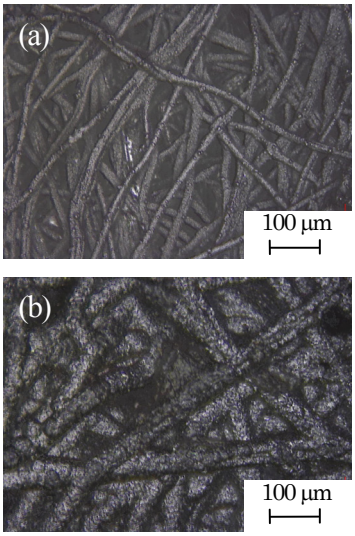

Fig. 6 Images of filter surface; (a) before deposition, (b) after deposition.

[Word Count] = (67+10)*2.2*1 + 12 (caption) = 182 words

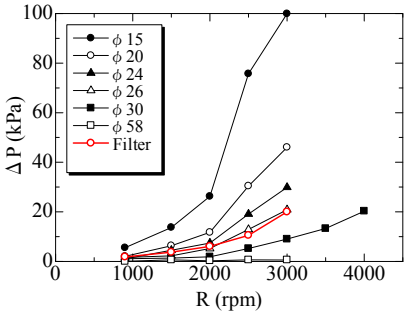

Fig. 7 Backpressure equipped with packing with different orifice diameter or filter.

[Word Count] = (40+10)*2.2*1 + 12 (caption) = 122 words

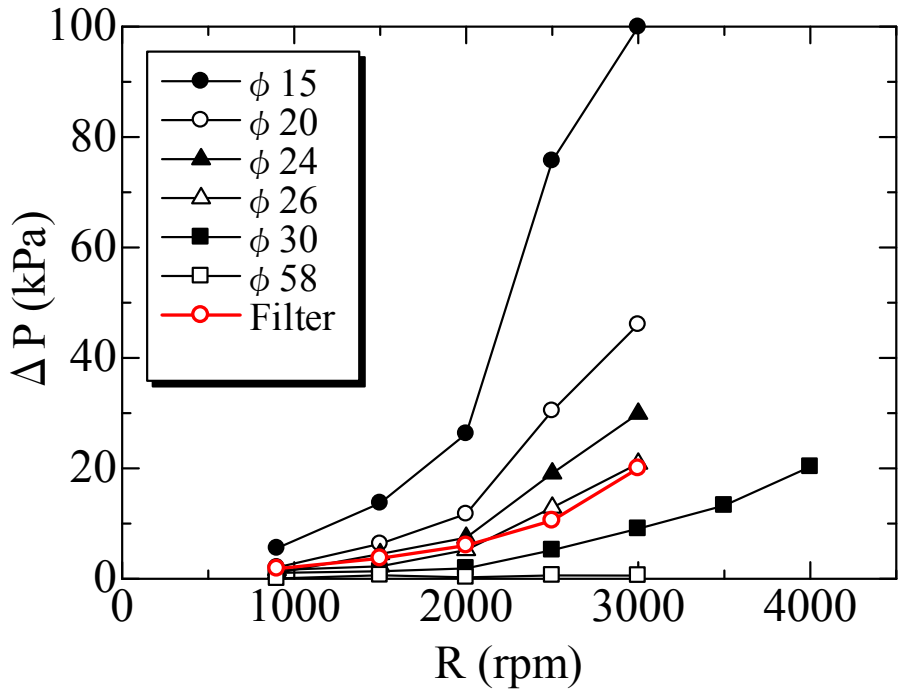

Fig. 7 (enlarged)

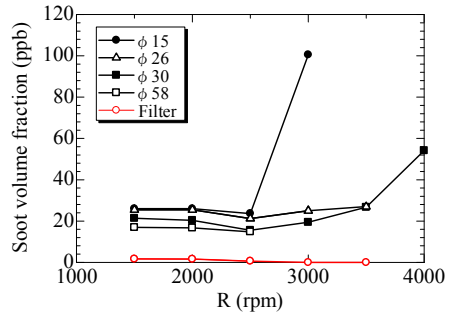

Fig. 8 Soot volume fraction equipped with packing with different orifice diameter or filter.

[Word Count] = (40+10)*2.2*1 + 13 (caption) = 123 words

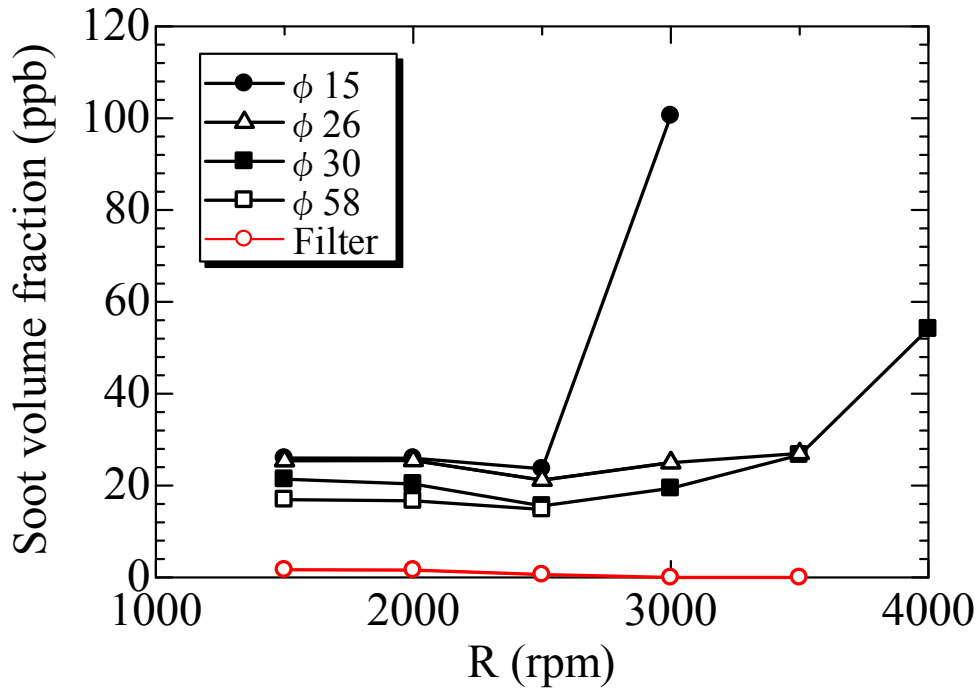

Fig. 8 (enlarged)

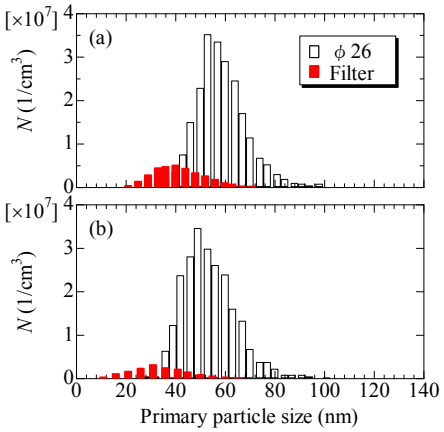

Fig. 9 Particle size distributions of primary soot equipped with packing with ϕ26 or filter; (a) R=1500 rpm, (b) R = 2500 rpm.

[Word Count] = (55+10)*2.2*1 + 23 (caption) = 166 words

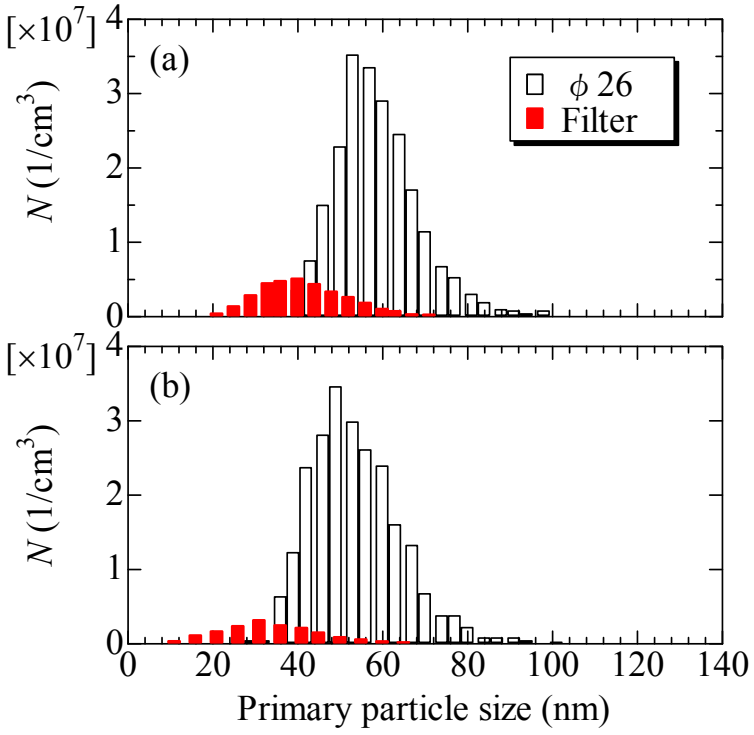

Fig. 9 (enlarged)

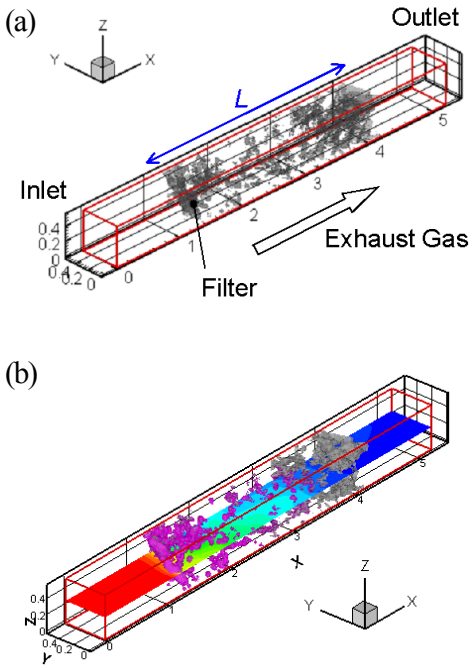

Fig. 10 (a) Computational domain with coordinate system, (b) 3D distribution of deposited soot inside filter. Profile in *x*-*y* plane expresses distribution of soot mass fraction in gas phase. Purple color-shaded contour expresses deposited soot. Gray contour expresses filter.

[Word Count] = (86+10)*2.2*1 + 39 (caption) = 250 words

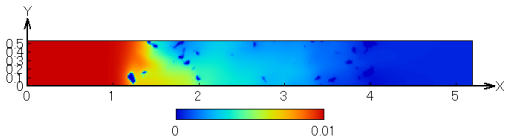

(a) Y_{Cg}

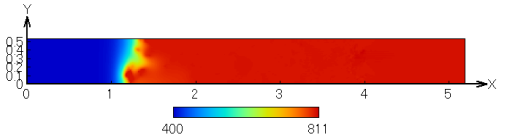

(b) T (°C)

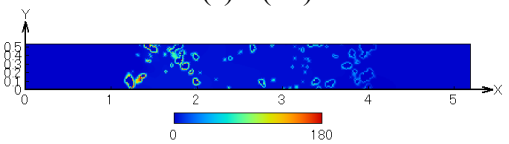

(c) W_C (kg/m^{3}s)

Fig. 11 Distributions of (a) soot mass fraction in gas phase, (b) temperature, (c) reaction rate; T_w=700℃.

[Word Count] = (75+10)*2.2*1 + 20 (caption) = 207 words

(a)

(b)

(c)

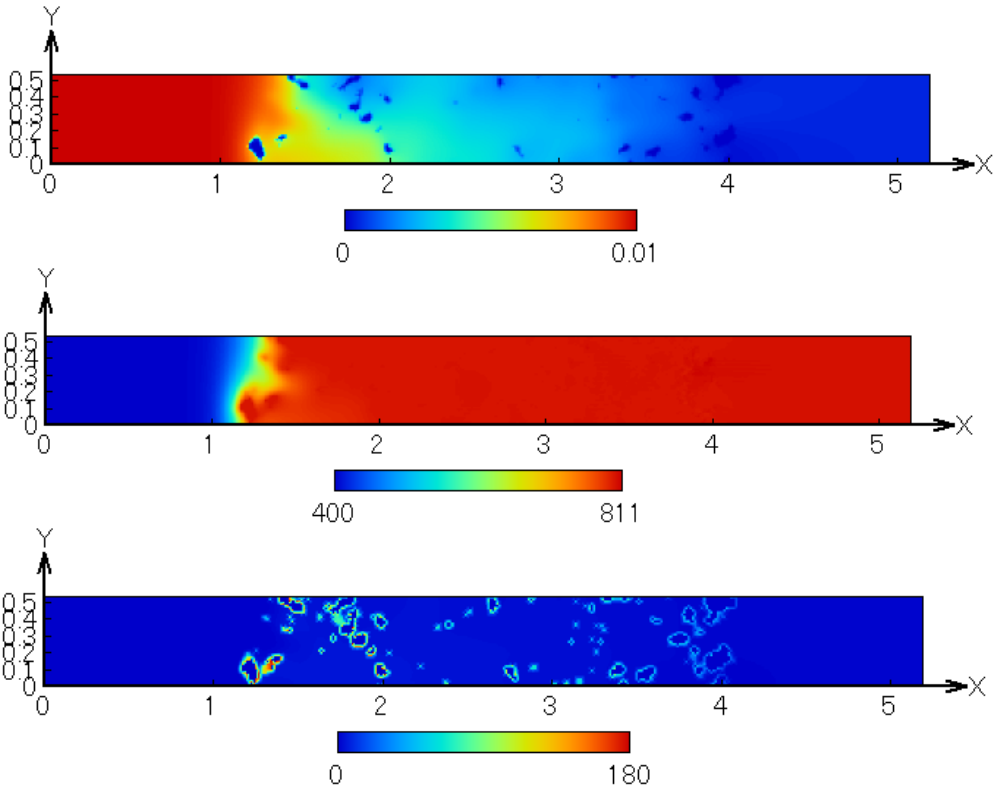

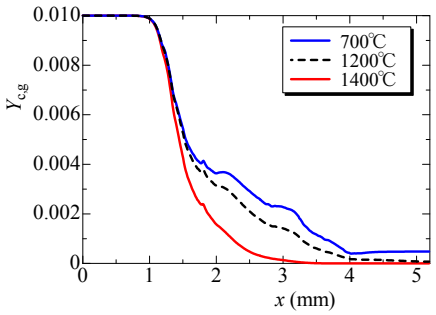

Fig. 12 Distributions of deposited soot at T_w=700, 1200, 1400℃.

[Word Count] = (40+10)*2.2*1 + 12 (caption) = 122 words

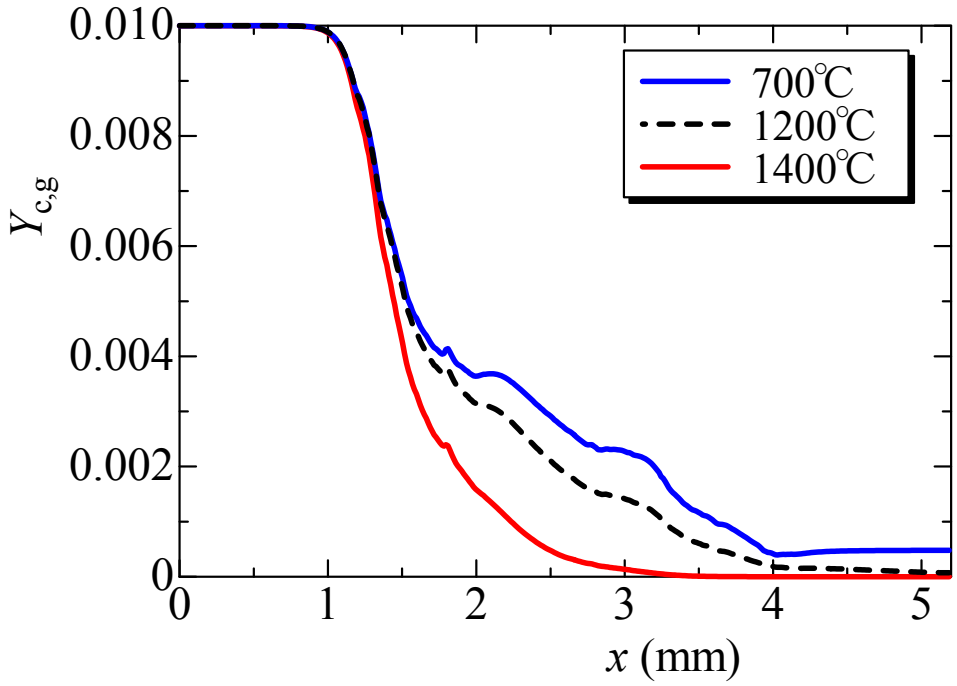

Fig. 12 (enlarged)